



# Intelligent robotic walker with actively controlled human interaction

Ihn-Sik Weon<sup>1</sup>  | Soon-Geul Lee<sup>2</sup> 

<sup>1</sup>Department of Mechanical Engineering, Graduated School, Kyung Hee University, Yongin, Rep. of Korea.

<sup>2</sup>Department of Mechanical Engineering, Kyung Hee University, Yongin, Rep. of Korea.

## Correspondence

Soon-Geul Lee, Department of Mechanical Engineering, Kyung Hee University, Yongin, Rep. of Korea.  
Email: sglee@khu.ac.kr

## Funding information

Korea Health Industry Development Institute (KHIDI); Ministry of Health & Welfare, Rep. of Korea, Grant/Award Number: HI15C1027; Agency for Defense Development.

In this study, we developed a robotic walker that actively controls its speed and direction of movement according to the user's gait intention. Sensor fusion between a low-cost light detection and ranging (LiDAR) sensor and inertia measurement units (IMUs) helps determine the user's gait intention. The LiDAR determines the walking direction by detecting both knees, and the IMUs attached on each foot obtain the angular rate of the gait. The user's gait intention is given as the directional angle and the speed of movement. The two motors in the robotic walker are controlled with these two variables, which represent the user's gait intention. The estimated direction angle is verified by comparison with a Kinect sensor that detects the centroid trajectory of both the user's feet. We validated the robotic walker with an experiment by controlling it using the estimated gait intention.

## KEYWORDS

2D-LiDAR, cyber physic sensor, gait intention, human-robot interactive, robotic walker

## 1 | INTRODUCTION

Recent medical technology developments and enhanced quality of life have improved public health, thereby creating an aging society with a high life expectancy [1]. However, daily life activities cannot be guaranteed for the elderly because of degenerative diseases, reduced motor ability, and low physical strength [2]. Among these factors, diminished muscle strength in the lower extremities results in gait instability [3]. Thus, gait orthosis is generally employed to assist patients' gait [4].

Most existing gait orthoses are manually operated and convenient to use owing to their intuitive operation. However, moving upward on a sloping path without separate power assistance in addition to their willpower and depending only on gait orthosis is difficult for elderly people. Thus, various interface-added gait orthoses should be employed [5].

PAM-AID is a contact-based interface developed by Trinity College. The device controls a robot with a bicycle-like

handle, as shown in Figure 1A [6]. The driving part in PAM-AID is controlled through a force sensor attached to the handle proportional to the force magnitude in both hands.

JAIST also determines the gait intention through various distance measurement sensors and the handle bar, as shown in Figure 1B [7,8]. Researchers from Carnegie Mellon University applied a haptic device to the handle of a walker to determine the user's gait intention and searched the surroundings using a two-dimensional (2D) laser range finder (LiDAR) [9]. However, the device could not fully determine gait intention based on the user's grip power and skill level [10]. Many studies have been conducted to improve the operation convenience of walkers through sensor convergence and steering improvements, and thus overcome said problems; however, the proposed methods are limited because vehicle control based on intention determination can only be achieved through the determination of accurate intention, as most are dependent on steering devices [11].

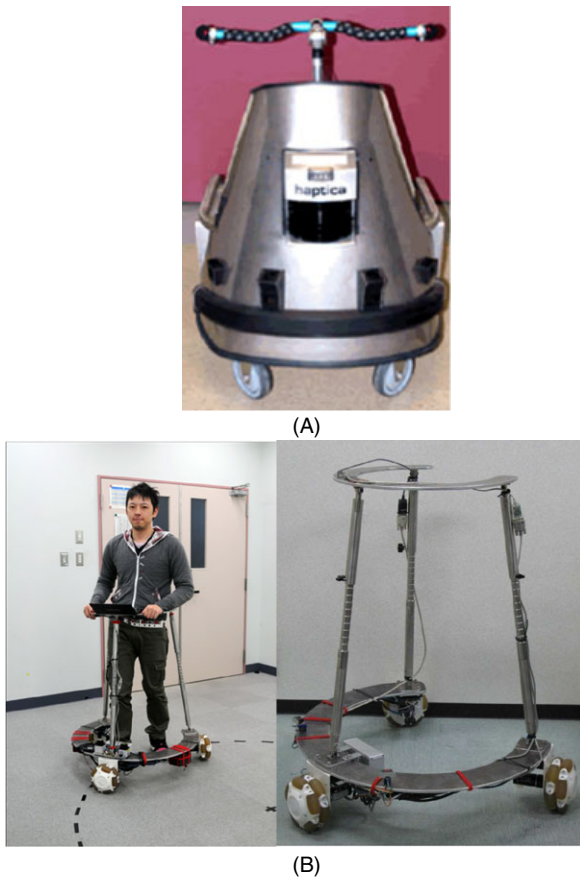


**FIGURE 1** Different types of robotic walkers: (A) VA-PAM-AID robotic walker and (B) JAIST active robotic walker (JARoW)

The platform-based contact-type interface cannot completely determine pedestrian or user intention. Hence, Yuan attached inertia sensors at the feet, shanks, thighs, and pelvis, and installed a force-sensing resistor (FSR) on the soles to detect contact between the feet and ground surface [12]. Through the study, he solved the problem of lower-extremity kinematics from the sole to the pelvis, which has an arbitrary ground contact position, by estimating the user's position and velocity [13]. Contact between the feet and ground surface must be detected to estimate the location and velocity of a pedestrian based on lower extremity kinematics [14–16]. Pappas and Park [17] installed an FSR and gyroscope to the soles of the shoes to detect contact between the feet and ground surface [18]. However, if FSRs or pressure sensors with inertia sensors have been used to detect contact between the feet and ground surface to solve the problem of lower extremity kinematics, then the system complexity increases as a result of changes in sensitivity due to differences in individual foot size and robustness owing to repetitive weight support [19]. A hidden Markov model can be used to analyze a three-dimensional gait motion using image sensors; however, this model is inferred in the discrete state space, which results

in significant information loss and decreased modeling accuracy [20,21].

The present study configures a contactless interface based on the determined user-oriented gait trajectory, gait-assistive platform, gait direction, and straightness gait intention. The knee joint movement according to the user's gait is extracted in the XY coordinates using a low-cost 2D LiDAR. A region of interest is set in the extracted distributed knee data and changes in the coordinate values for the gait state of both feet acquired over time are classified into mean data, and the heading angle of the moving trajectory in the coordinate values is therefore calculated.

The system derives correlations using the covariance, correlation, and coefficient along with the heading angle information on position data from the heading angle calculated based on knee movement. Furthermore, the system extracts knee data of the pedestrian's lower body in the form of XYZ coordinate information from the image data of the pedestrian's lower body. The system calculates the centroid of the three-axis coordinate system in the lower body in accordance with the pedestrian's movements. Moreover, the system compares two sets of data to generate the coefficient that determines gait intention [1].

## 2 | MATERIAL AND METHODS

### 2.1 | Hardware system description

A low-cost LiDAR sensor that is driven by a servomotor in the moving platform is used to calculate indirect gait intention of the pedestrian. Two nine degree-of-freedom inertia measurement unit (IMU) sensors are attached to both feet of the pedestrian [22]. The LiDAR sensor installed in the moving platform is an LiDAR-Lite2 product from pulsed light; the distance error is  $\pm 0.025$  m, and the cycle is 50 Hz.

The interface is configured through the inter-integrated circuit communication with a sub controller, and the sensor's vertical distance is measured in accordance with the servomotor's movements.

As shown in Figure 2, a 2D LiDAR sensor is mounted on the servomotor to detect the distance region equal to the determined space. The LiDAR sensor using the servomotor detects the distance value that is equal to a  $30^\circ$  region. The detection cycle is set to 100 Hz through the micro-controller and an actual gait cycle is assumed to be the mean gait cycle of 1.2 m/s–1.6 m/s to extract pedestrians' knee data depending on their movements [24–25]. In addition,  $x$ -imu sensors are attached to the toes of both feet of the pedestrian. These inertial sensors transmit data at 115,200 bytes per second through a USB-RS232 mode, which is the same mode used in the micro-controller. In addition, 2D-LiDAR data are synchronized with data of the laptop, a higher-level controller, to receive walking motion data [26].

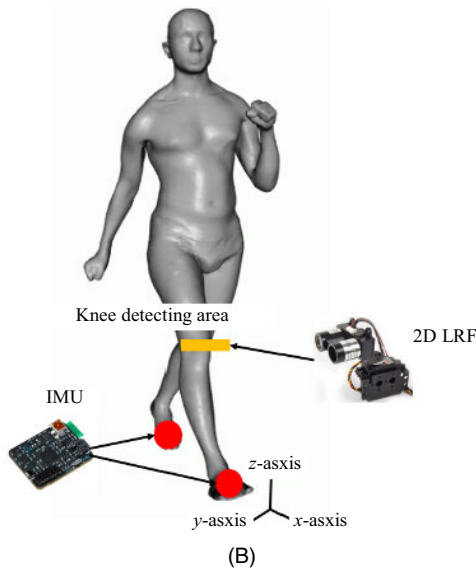
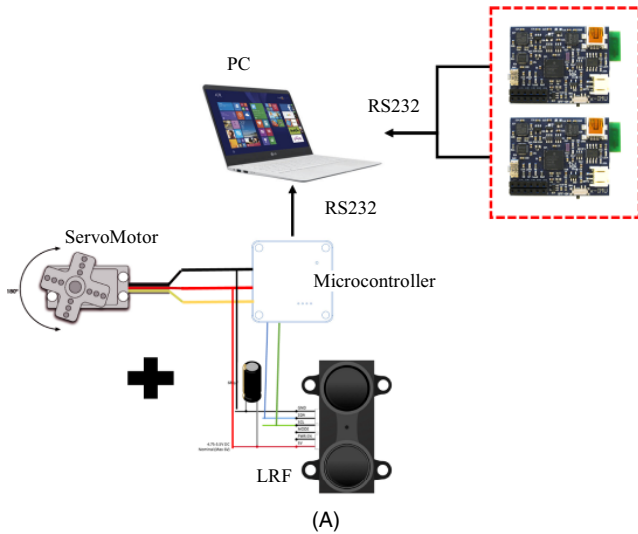


**FIGURE 2** System configuration of the gait analysis: (A) system configuration and (B) configuration of a gait intention device system

## 2.2 | Mathematical background

### 2.2.1 | Motion model

XYZ coordinates represent the dynamic equation according to the user's gait, which includes gait velocity and location characteristics. Given that an inertial sensor cannot find its own absolute coordinate values, it should conduct an initial correction. Equation (1) shows the acceleration of a moving body at the initial state in the inertial sensor [27].

As presented in (1), acceleration at  $X$  and  $Y$  is 0 in the stationary state and can be expressed as  $f^n = [0, 0, -g^n]^T$ . The initial coordinate transformation matrix can be expressed as  $C_b^n$  in (2) as a Eulerian angle where  $\Phi$  is the roll angle,  $\theta$  is the pitch angle, and  $\Psi$  is the yaw angle.

$$f^n = [f_x f_y f_z] = \begin{bmatrix} \sin \theta g^n \\ -\sin \Phi \cos \theta g^n \\ -\cos \Phi \cos \theta g^n \end{bmatrix}, \quad (1)$$

$$C_b^n = \begin{bmatrix} \cos(\theta) \cos(\psi) \sin(\Phi) \sin(\theta) \cos(\psi) - \cos(\Phi) \sin(\psi) \\ \cos(\theta) \cos(\psi) \sin(\Phi) \sin(\theta) \cos(\psi) + \cos(\Phi) \sin(\psi) \\ -\sin(\theta) & \sin(\Phi) \cos(\theta) \\ \cos(\Phi) \sin(\theta) \cos(\psi) - \sin(\Phi) \sin(\psi) \\ \cos(\Phi) \sin(\theta) \sin(\psi) - \sin(\Phi) \cos(\psi) \\ \cos(\Phi) \sin(\theta) \end{bmatrix}, \quad (2)$$

$$V^n = C_b^n f^n - (2\omega_{ie}^n + \omega_{en}^n) \times V^n + g^n. \quad (3)$$

Location and velocity are obtained by calculating a navigation equation after converting the acceleration  $f^n$  in the navigation coordination system of the moving body in the coordinate transformation matrix  $C_b^n$ . The velocity can be calculated using (3) [28].  $V^n$  refers to a component of the velocity represented in the navigation coordinate system,  $\omega_{ie}^n$  refers to the angular velocity with regard to the inertial coordinate system in the navigation coordinate system, and  $\omega_{en}^n$  refers to the angular velocity with regard to the inertial coordinate system in the Earth-fixed coordinate system [29].

$$\omega_{ie}^n = [\Omega \cos \bar{X}, 0, -\Omega \sin \bar{X}], \quad (4)$$

$$\begin{aligned} \omega_{en}^n &= [\rho_X, \rho_Y, \rho_Z] = [\bar{Y} \cos \bar{X}, -\bar{X}, \bar{Y} \sin \bar{X}] \\ &= \begin{bmatrix} \frac{V_E}{(R_0 + h)} & -\frac{V_N}{(R_0 + h)} & -\frac{V_E \tan \bar{X}}{(R_0 + h)} \end{bmatrix}^T, \end{aligned} \quad (5)$$

$$R_m = \frac{R_0(1 - e^2)}{(1 - e^2 \sin^2 \bar{X})^{3/2}}, \quad (6)$$

$$R_t = \frac{R_0}{(1 - e^2 \sin^2 \bar{X})^{1/2}}. \quad (7)$$

In the above equations,  $R_0$  is the radius of the equator of the Earth ellipsoid,  $e$  is the Earth eccentricity, and  $\Omega$  is the angular velocity of the Earth's rotation;  $h$  is the height of the body and  $L$  is the latitude.

In the above equations, the superscripts indicate the frame in which each vector is expressed, and  $V^n = [V_x, V_y, V_z]^T$  is the velocity vector on the navigation frame [34–36].

$$\bar{X} = \frac{V_x}{R_L + h}, \bar{Y} = \frac{V_y}{(R_t + h) \cos L}, \bar{Z} = -V_z. \quad (8)$$

By integrating (8), the velocity and position of the navigation frame can be obtained.

## 2.2.2 | Calculated XYZ coordinates from 2D-LiDAR

A laser scanner method using the phase difference generates electric signals by reflecting the laser phase and intensity. The sensor compares the phase intensities between the initial launch signal and returned signal to measure the distance.

$$L = \frac{1}{2} \times \left( \frac{\theta}{\left(\frac{f}{c} \times 2\pi\right)} \right). \quad (9)$$

In (9),  $L$  is the distance to the target,  $\theta$  is the phase difference,  $f$  is the laser frequency, and  $c$  is the speed of light. Furthermore, the coordinate system of an object in 2D space can be created with distances and angles extracted by the laser scanner. Equation (9) shows the calculation of the 2D coordinate system generation. The extraction region of the laser scanner is  $90^\circ$  to  $120^\circ$ , and  $h$  is the laser scanner's mounted height. Hence, (10) allows us to extract a pedestrian's knee data from the coordinate system.

$$O_{\text{LRF}} - \text{XYZ} = \begin{bmatrix} L \times \sin \theta \\ L \times \cos \theta \\ h \end{bmatrix}. \quad (10)$$

## 3 | GAIT TRACKING ALGORITHM

### 3.1 | Gait heading detection

The heading angle for each location is monitored using gait trajectories collected through the IMU sensor to analyze a pedestrian's movement. Moreover, the degree of knee movement is averaged using a 2D-distributed coordinate system knee data acquired from the laser scanner. The resulting data are created as a single-vector coordinate system and then calculated and derived as a heading angle over time.

#### 3.1.1 | Measured heading from dead reckoning

A low-cost nine-axis IMU sensor monitors the pedestrian's toe movements, acceleration, angular velocity, and geomagnetic output values obtained from the IMU sensor determine the pedestrian's direction and movement through an extended Kalman filter based on quaternion. Moreover, the velocity error of a pedestrian determined through the Kalman filter is corrected through zero velocity updating. The determined data are calculated with three-axis data that include direction and velocity.

In the location coordinates of the gait trajectory over time calculated with the three-axis coordinate system, the

heading angle rate with regard to the current data is calculated using the previous data location at time  $t$  and location  $t + 1$ , as shown in Figure 3. The calculated angle rate is  $\dot{\theta}_{\text{IMU}}(t)$ , and this is constant for a straight gait. However, when the gait direction changes,  $\dot{\theta}_{\text{IMU}}(t)$  is constantly directed in a certain direction.

#### 3.1.2 | Measured heading from the knee XYZ coordinates

The 2D data of the coordinate system in the space inside the platform—including knee data—are extracted using the LiDAR installed in the platform. Thereafter, a region of interest (ROI) is extracted as shown in Figure 4; it is obtained with the LiDAR when its position is initialized. After that, the two motion data are divided by the distance based on two feet with respect to the virtual baseline. The knee data  $P_1(x_1, y_1)$ ,  $P_2(x_2, y_2)$  in both feet divided by the virtual region and line are the means  $P_{\text{avg}}(x, y)$  of the distributed data, which generate point data. The direction is also determined according to how much the point data move.

### 3.2 | Gait intension prediction algorithm

The point data between two legs extracted using the platform determine the right or left direction through angle calculation and origin point data coordinates in the LiDAR. Moreover, the correlation between data is calculated with

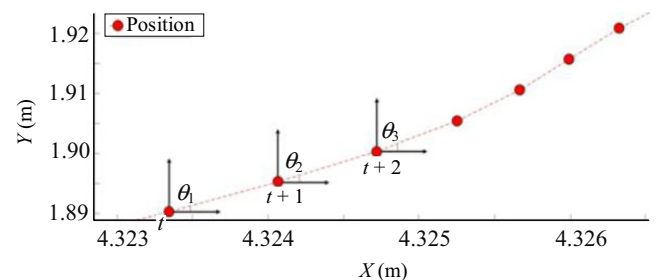


FIGURE 3 Gait analysis with position estimation data

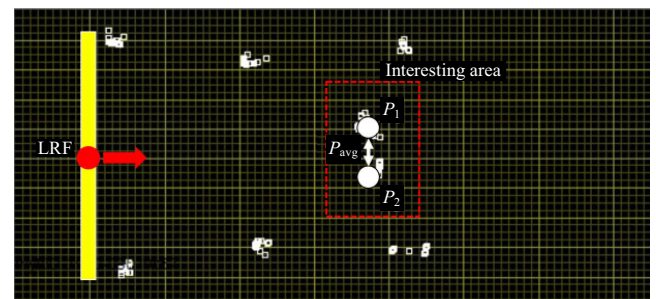


FIGURE 4 2D coordinate generated by low-cost LiDAR



the heading angle of the pedestrian's gait trajectories generated by the IMU sensor. The values between the two legs are compared as shown in Figure 4, thereby creating movement coordinates for the knees.

$$P_{avg} = \left( \frac{x_1 + x_2}{2}, \frac{y_1 + y_2}{2} \right). \quad (11)$$

Figure 5 shows the flowchart of the algorithm that extracts knee information from the LiDAR. Values according to the angles where the movement of both legs can be extracted from the LiDAR are received as raw data, and a virtual region of interest is made to extract only the data of both legs because large amounts of unnecessary data—including for the moving platform—are included in the received data.

The two feet are divided by creating a virtual centerline and a center mean point for the knees based on the boundary line. If the point of both legs is not extractable here, then data generated previously by dividing a region are detected and another value is extracted. As in (11), the calculated mean value  $P_{avg}(t)$  of both legs creates a heading angle according to time through the internal angle calculation with  $P_{avg}(t + 1)$ . The created heading angle is constantly calculated according to time and the pedestrian's gait direction is determined based on the heading angle's positive or negative direction.

In Figure 5, gait intention can be determined using the heading angle over time created by the IMU. The heading angle is correlated with the calculated LiDAR data  $\theta_{LRF}$ , thereby the correlation between  $\theta_{LRF}$  and  $\theta_{IMU}$  is determined.

Figure 6 shows how the heading angle derived through the inertial sensor calculates the internal angle between the

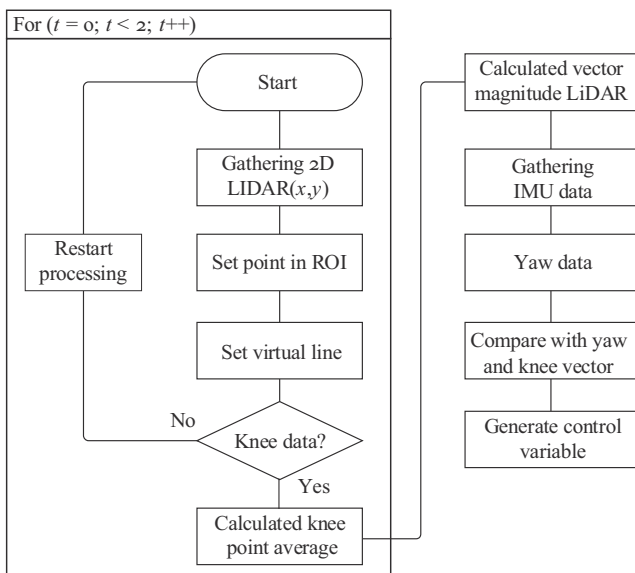


FIGURE 5 Flowchart for the intention variable with the LiDAR

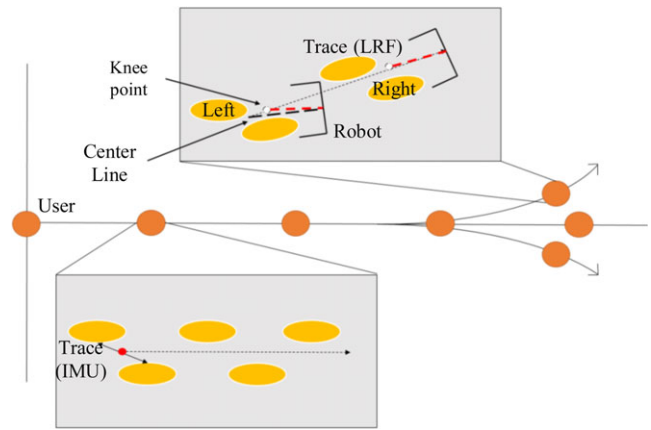


FIGURE 6 Gait tracking with knee detection data and the IMU

updated data, but the heading angle calculated based on the knee determines the internal angle with the mean point of both feet based on the LiDAR mounted on the gait-assistive robot. Thus, the heading angle calculated through the IMU shows a clear gait cycle pattern. However, the results from the LiDAR reveal a change in the angle when the direction changes and no change is found after the heading angle is perpendicular to the gait-assistive robot. Therefore, there is correlation between the heading angles when the direction between the two sets of data differs.

### 3.3 | Comparison with the vision system

Pedestrians' gait intention is determined using a Kinect SDK v1.0 from Microsoft to calculate the centroid of pedestrian movements in the lower extremities, including the knees, through image sensors, as shown in Figure 7. The trajectory data of centroid information show a similar pattern to that of the results created using the inertial sensor, and the image sensor lets us calculate the distance between the legs. The trajectory compares the heading

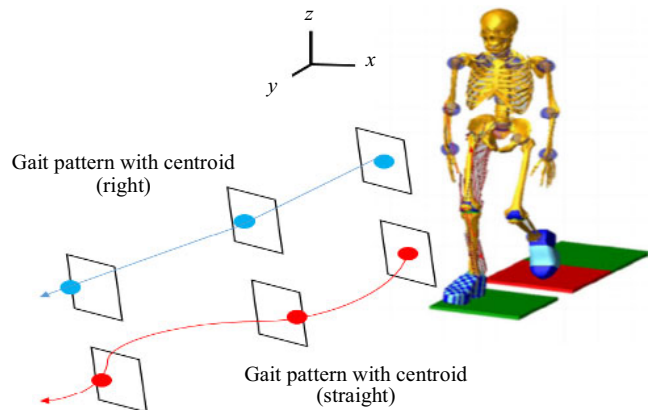


FIGURE 7 Gait pattern with centroid using a Kinect sensor [15]

angle information of gait intention determined using the IMU and LiDAR [30].

## 4 | EXPERIMENT AND RESULTS

We conducted the gait intention detecting experiment in the hallway of a normal office building while a user walked or moved in a pre-set range where the range and trajectory are set in advance. The following three motion scenarios were used to test the gait intention of direction detection:

- (1) Straight walking: The user walks straight forward for four steps with a stride of 134 cm.
- (2) Right-turn walking: The user folds to the right side at  $10^\circ$  intervals around the point of completing the four steps of straight walking gait.
- (3) Left-turn walking: The user walks on the left side in the same manner as in (2).

The distance between the gait orthosis mounted with LiDAR and Kinect sensors and the user is maintained at 35 cm, as shown in Figure 8.

### 4.1 | Gait intention detection with gait data

Only the direction intention between the two sets of knee data is measured using the gait direction extracted from the knee data of the gait trajectory.

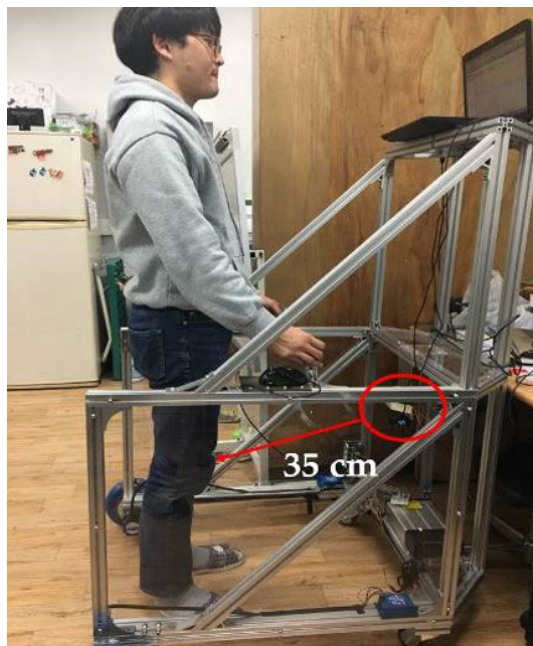


**FIGURE 8** Experiment setup: distance configuration between a user and the LRF sensor of the prototype rollator

As shown in Figure 9, the direction intention for the gait can be determined by the knee movement measured with the LiDAR. The center of the body can be expressed as the middle point of both knees based on a virtual line. When the user turns to a preferred direction with a change in the heading angle, the knees also change to that direction consistently beyond the virtual centerline. Figure 9B shows how the left knee crosses over the centerline in the Y-axis when the user turns right. Conversely, Figure 9C shows that the knees turn left when the user turns left.

Figure 10 shows the change in the vector between the robotic walker and the user's knees during left-turn walking. The data only show one cycle of a typical gait. Figure 10 shows that the deviation is in the range  $-0.2$  to  $0$ . Before the users change their walking direction to the right or left, they usually turn their bodies in that direction and push the robotic walker in that direction. The vertical distance increases and the deviation becomes greater than that in existing data, as shown in Figures 11 and 12. The change in the vector with respect to the virtual line during user's gait clearly shows the characteristics of the walking intention as shown in the figures. As the user turns to a certain

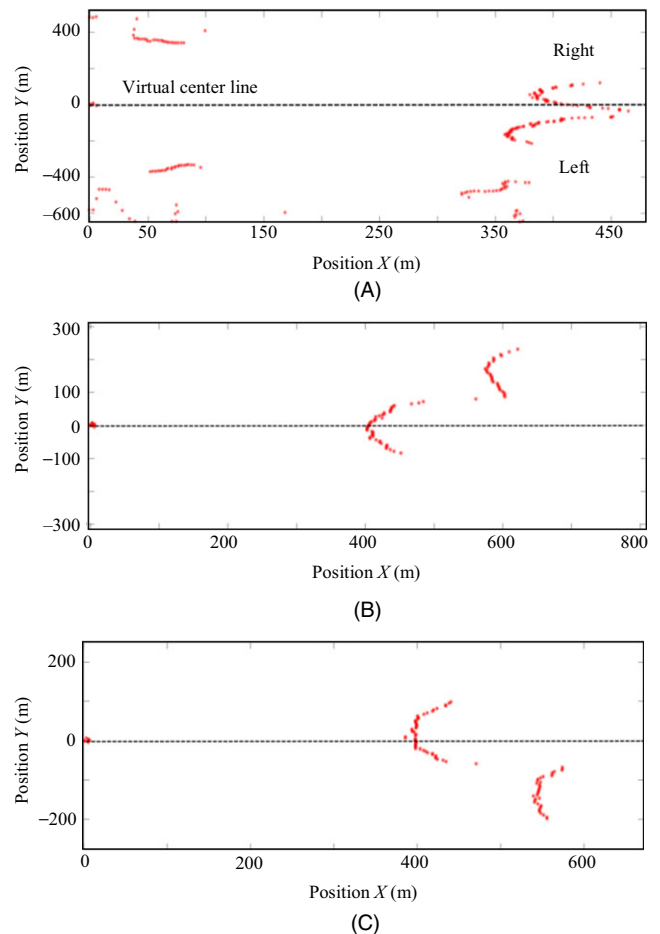


**FIGURE 9** Gait tracking with knee detection: (A) straight walking, (B) right-turn walking, and (C) left-turn walking

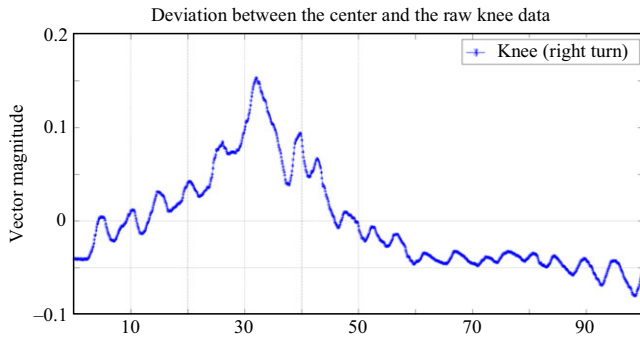


**FIGURE 10** Gait tracking variation in knee detection during right-turn walking

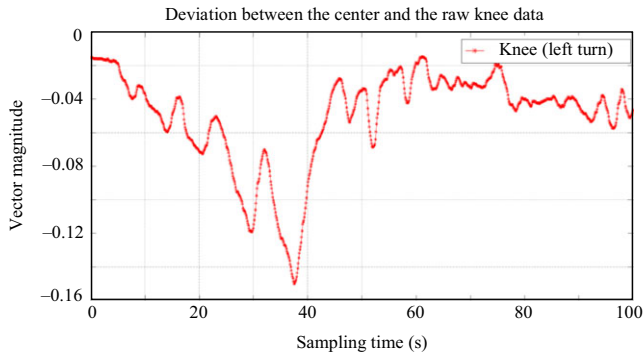


**FIGURE 11** Gait tracking variation in knee detection for left-turn walking

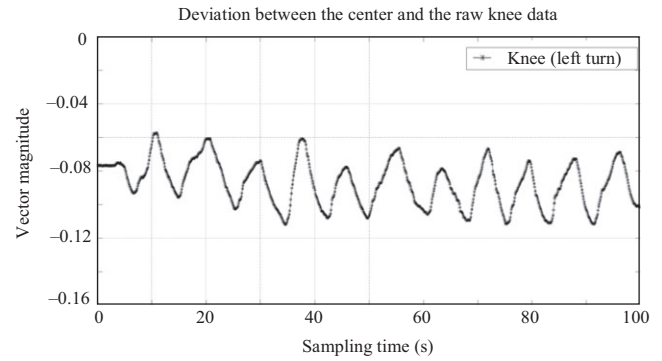
direction, the deviation from the virtual center line along the Y-axis increases depending on the change in distance.

Figure 10 shows the obtained data during right-turn walking where the positive vector magnitude denotes the deviation of the middle position of both knees from the virtual center line to the right. Figure 11 shows that there is an overall tendency of moving left as a downward curve until 38 seconds, but the short-term data pattern shows a swaying motion.

Figure 12 shows the obtained data for straight walking. The data fluctuate left to right for each gait cycle, but the average value of each gait cycle remains within a threshold level, shown as the dotted line in Figure 12.

For both right-turn and left-turn walking, the heading angle of walking is measured with IMU sensors attached to each foot as shown in Figure 13. The trend of the point location data generated with the assumption that the turning point after straight walking ends is (0, 0), as shown in Figure 14. A significant amount of noise can be found in the gait direction data as the movement degree in the knees in a limited virtual space is measured through the LiDAR; however, the gait trend can be identified.

Figure 15 shows how the angles generated during right walking based on the starting point can be calculated as an absolute value. The accurate heading angle is calculated through comparison with the gait direction calculated



**FIGURE 12** Gait tracking variation in knee detection for straight walking

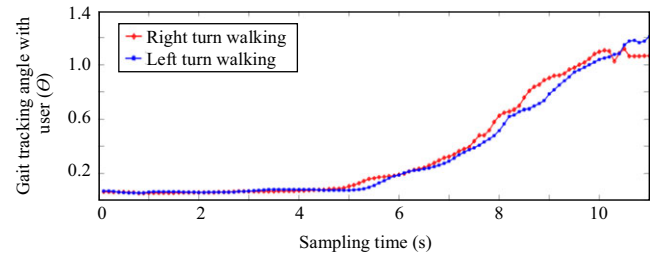


**FIGURE 13** Heading angle of left-turn and right-turn gait (IMU)

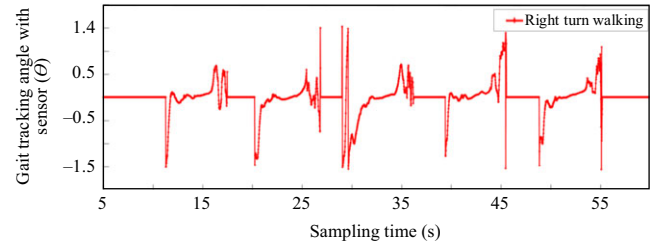


**FIGURE 14** Angle of gait tracking by a fusing algorithm

through the LiDAR, as shown in Figure 15. Figure 13 shows a regular pattern of the heading angle rate measured with the movement point data for each case. The deviation for the left-turn and the right-turn gait is more severe than that for the straight gait. Figure 14 shows the angle of gait tracking by fusing algorithm results obtained from the inertial sensor and the LiDAR. These results are similar to those extracted for the knees, but a significant deviation between the two sets of data calculated using Figure 15 is found during the direction-change gaits. Moreover, the heading angle from the knees is  $3^\circ$  through  $5^\circ$ , whereas the data obtained through the IMU indicate that the maximum change angle per gait cycle is  $2^\circ$  with a  $1^\circ$  through  $3^\circ$  error.

## 4.2 | Controlled direction of robotic walker

The robot walker is driven using the walking intention variables, and the experiment is conducted for three types of movement: straight walking, left-turn walking, and right-

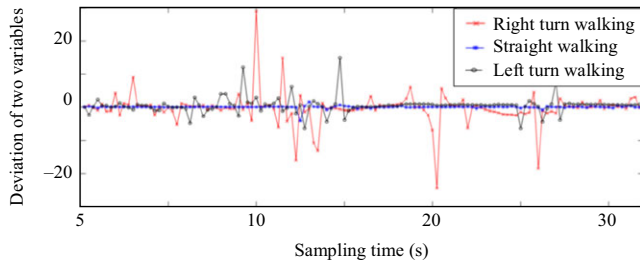


**FIGURE 15** Deviation between the centroid (vision) and the fused data with LRF and IMU

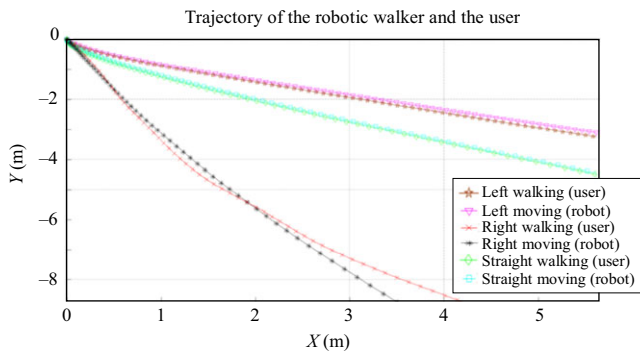


**FIGURE 16** Heading angle of left-turn and right-turn gait (IMU)

turn walking. Non-contact determination for gait intention is performed using the LiDAR and IMU sensors. Then, even if the user does not hold it, the walking-assist robot can move in the walking direction the users intend.

In the case of the straight walk in Figure 16, as the user keeps a regular walking pattern, the walking-assist robot also follows the straight walking as well. In the case of the right-turn or left-turn walking in Figure 16, the angle of the detected direction is larger than that of the user's moving direction. In particular, in the case of right turning, the walking assist robot moved  $5^\circ$  further than the user's walking intention. One reason for this is that the experiment was performed by setting the angle according to the fixed threshold value and the walking intention without considering each case's gait characteristic.

## 5 | DISCUSSION

Algorithm data are tracked to track progression through the knee joint's kinematic trajectory; this generates a phase relationship between the two sets of data by using the algorithm of the data that proceeds through each inertial sensor. The actual walking direction is estimated using the correlation data. In particular, the results verify that  $1^\circ$  to  $2^\circ$  of turning from the center point occurs in every cycle when the pedestrian turns right or left, as shown in Figure 15. The present study results are compared with other study results on gait intention determination that are obtained by

calculating the centroid of lower-extremity joints through Kinect. Consequently, there is a large deviation in terms of walking in a certain direction. However, this limitation can be overcome by employing a dynamic mechanism analysis of pedestrians and a walking-assistive robot.

## 6 | CONCLUSION

The present study investigated user movement in a virtual space where a walking-assistive robot moves to generate movements with 2D coordinates. In particular, the movement trajectories of knee joints and toes in the current study are generated using the heading angles of data over time such that the directions taken by pedestrians are expressed as gait intention. The current results are compared with those of other studies on gait intention that utilize existing image sensors. Notably, the present findings can identify gait intention trends. Considering a gait with approximately  $14^\circ$  turning from the starting line, three gait cycles with  $1^\circ$  to  $3^\circ$  of turning for each are determined, which can ultimately identify the gait heading angle and intention. However, this can create a maximum error of up to 30 cm; this error is relatively large compared to data obtained from the image sensor. Nonetheless, we can reduce this through future gait intention studies that include gait-oriented mechanical analysis and the mechanical analysis of walking-assistive robots. Therefore, the present findings lay a foundation for further exploration of the driving control of walking-assistive robots.

## ACKNOWLEDGEMENTS

This research was supported by the Korea Health Industry Development Institute (KHIDI), funded by the Ministry of Health & Welfare, Republic of Korea (grant number: HI15C1027), and Agency for Defense Development under the contract 20170859.

## ORCID

Ihn-Sik Weon  <http://orcid.org/0000-0003-0452-7056>

Soon-Geul Lee  <http://orcid.org/0000-0002-4588-6736>

## REFERENCES

1. K. Sagawa et al., Unrestricted measurement method of three-dimensional walking distance utilizing body acceleration and terrestrial magnetism, *Int. Conf. Contr. Autom. Syst.*, Jeju Island, Rep. of Korea, 2001, pp. 707–710.
2. V. Gabaglio et al., Centralised Kalman filter for augmented GPS pedestrian navigation, *ION GPS 2001*, Salt Lake City, UT, USA, Sept. 11–14, 2001, pp. 312–318.



3. A. Sinha et al., Person identification using skeleton information from Kinect, *Int. Conf. Adv. Computer-Human Interactions*, Nice, France, 2013, pp. 101–108.
4. Q. Ladetto, On foot navigation: Continuous step calibration using both complementary recursive prediction and adaptive Kalman filtering, *Proc. Int. Techn. Meeting Satellite Division Institute Navigation*, Salt Lake City, UT, USA, Sept. 19–22, 2000, pp. 1735–1740.
5. S. H. Shin, MEMS-based personal navigator equipped on the user's body, *Int. Techn. Meeting Satellite Division*, Long Beach, CA, USA, Sept. 13–16, 2005, pp. 1998–2002.
6. B. K. Sin, Parallel Gaussian processes for gait and phase analysis, *J. KHSE*. **42** (2015) no. 6, 748–754.
7. G. Lee et al., JAIST robotic walker control based on a two-layered Kalman filter, *IEEE Int. Conf. Rob. Autom. (ICRA)*, Shanghai, China, May 9–13, 2011, pp. 3682–3687.
8. G. Lee et al., Walking intent-based movement control for JAIST active robotic walker, *IEEE Trans. Syst. Man, Cybernetics: Syst.* **44** (2014), no. 5, 665–672.
9. J. Pineau et al., Towards robotic assistants in nursing homes: Challenges and results, *Robotics Autonomous Syst.* **42** (2003), no. 3–4, 271–281.
10. Motion Capture Camera, 2015, available at <http://www.vicon.com>.
11. K. Aminian et al., Level downhill and uphill walking identification using neural networks, *Electron. Lett.* **29** (1993), no. 17, 1563–1565.
12. X. Shao et al., Analyzing pedestrians' walking patterns using single-row laser range scanners, *IEEE Int. Conf. Syst. Man Cybern.*, Taipei, Taiwan, Oct. 8–11, 2006, pp. 1202–1207.
13. J. Preis et al., Gait recognition with Kinect, *Int. Workshop Kinect Pervasive Comput.*, Newcastle, UK, 2012, pp. P1–P4.
14. I. S. Won et al., A study of a walking intention based on the 3D area and centroid of lower body using RGB-D, *Conf. Korea Soc. Precis. Eng.* **2016** (2016), no. 5, 262–263.
15. A. Mikov et al., A localization system using inertial measurement units from wireless commercial handheld devices, *IEEE Int. Conf. Indoor Position. Indoor Navigation (IPIN)*, Montbeliard, France, Oct. 28–31, 2013, pp. 1–7.
16. S. Rajagopal, Personal dead reckoning system with shoe mounted inertial sensors, MS. thesis, KTH Electrical Engineering, Stockholm, Sweden, 2008, pp. 1–45.
17. D. Roetenberg, H. Luinge, P. Slycke, MVN: Full 6DOF human motion tracking using miniature inertial sensors, *XSENS Technol.* **1** (2013), 1–9.
18. M. K. Kim, D. H. Lee, Research on the development of IMU based foot-ground contact detection (FGCD) algorithm in real-time with considering walking speed, *Conf. Korea Soc. Mech. Eng.* **2015** (2015), no. 11, 2822–2827.
19. C. A. Cifuentes et al., Human-robot interaction based on wearable IMU sensor and laser range finder, *Rob. Auton. Syst.* **62** (2014), no. 10, 1425–1439.
20. B. K. Santhiranayagam et al., Regression models for estimating gait parameters using inertial sensors, *IEEE Int. Conf. Intell. Sens. Sens. Netw. Inform. Process. (ISSNIP)*, Adelaide, Australia, Dec. 6–9, 2011, pp. 46–51.
21. R. Jirawimut et al., A method for dead reckoning parameter correction in pedestrian navigation system, *IEEE Instrum. Meas. Technol. Conf.*, Budapest, Hungary, May 21–23, 2001, pp. 209–215.
22. S. Y. Cho, Design of a pedestrian navigation system and the error compensation using RHKF filter, Ph.D. dissertation, Kwangwoon University, Seoul, Rep. of Korea, 2004.
23. R. Harle et al., A survey of indoor inertial positioning systems for pedestrians, *IEEE Commun. Surv. Tutor.* **15** (2013), no. 3, 1281–1293.
24. S. Godha et al., Integrated GPS/INS system for pedestrian navigation in a signal degraded environment, *Int. Technical Meetings Satellite Division Institute Navigation*, Fort Worth, TX, USA, 2006, pp. 2151–2164.
25. M. S. Lee et al., Evaluation of a pedestrian walking status awareness algorithm for a pedestrian dead reckoning, *Int. Techn. Meeting Satellite Division Institute Navigation*, Portland, OR, USA, Sept. 21–24, 2010, pp. 2280–2284.
26. O. Woodman, Pedestrian localisation for indoor environments, Ph.D. dissertation, University of Cambridge, 2010.
27. E. Foxlin, Motion tracking requirements and technologies, *Handbook of virtual environment technologies*, Lawrence Erlbaum Publishers, New Jersey, USA, 2002, p. 182.
28. J. O. Nilsson et al., Cooperative localization by dual foot-mounted inertial sensors and inter-agent ranging, *EURASIP J. Adv. Signal Process.* **2013** (2013), no. 1, 164:1–164:17.
29. J. Ballesteros et al., On gait analysis estimation errors using force sensors on a smart rollator, *Sensors* **16** (2016), no. 11, 1896:1–1896:15.
30. I. S. Weon et al., Estimation of walking intension using centroid variation of lower body area, *J. Korean Soc. Precis. Eng.* **34** (2017), no. 5, 323–329.

#### AUTHOR BIOGRAPHIES



**Ihn-Sik Weon** received his B.S. degree in mechanical engineering from the Engineering College, Korea University, Seoul, Rep. of Korea, in 2014, and his M.S. and Ph.D. degrees in mechanical engineering from the Engineering College, Kyunghee University, Yongin, Rep. of Korea. His main research interests are autonomous vehicle control algorithms, unmanned surface vessels, and intelligent assistance robots.



**Soon-Geul Lee** received his B.E. degree in Mechanical Engineering from Seoul National University, Rep. of Korea; an M.S. degree in Production Engineering from KAIST, Seoul, Rep. of Korea; and a Ph.D. degree in Mechanical Engineering from the University of Michigan in 1983, 1985 and 1993, respectively. Since 1996, he has been with the Department of Mechanical Engineering of Kyung Hee University, where he is currently a professor. His research interests include robotics and automation, mechatronics, intelligent control, and biomechanics.